



Engineered biochar from pine wood: Characterization and potential application for removal of sulfamethoxazole in water

Hyun Min Jang¹, Seunghyun Yoo², Sunkyu Park², Eunsung Kan^{1,3†}

¹Department of Agricultural and Biological Engineering & Texas A&M AgriLife Research Center at Stephenville, Texas A&M University, College Station, USA

²Department of Forest Biomaterials, North Carolina State University, Raleigh, USA

³Department of Wildlife, Sustainability, and Ecosystem Sciences, Tarleton State University, Stephenville, USA

ABSTRACT

The adsorption of sulfamethoxazole (SMX) onto a NaOH-activated pine wood-derived biochar was investigated via batch experiments and models. Surprisingly, the maximum adsorption capacity of activated biochar for SMX (397.29 mg/g) was superior than those of pristine biochars from various feedstock, but comparable to those of commercially available activated carbons. Elovich kinetic and Freundlich isotherm models revealed the best fitted ones for the adsorption of SMX onto the activated biochar indicating chemisorptive interaction occurred on surface of the activated biochar. In addition, the intraparticle diffusion limitation was thought to be the major barrier for the adsorption of SMX on the activated biochar. The main mechanisms for the activated biochar would include hydrophobic, π - π interactions and hydrogen bonding. This was consistent with the changes in physicochemical properties of the activated biochar (e.g., increase in sp^2 and surface area, but decrease in the ratios of O/C and H/C).

Keywords: Activated biochar, Antibiotics, Sulfamethoxazole (SMX), Water treatment, π - π interaction

1. Introduction

Various pharmaceutical compounds released to environments have attracted rising attention due to their adverse effects such as endocrine disruption and prevalence of antibiotic resistance genes [1]. According to recent literatures [2], the low metabolic rates of many pharmaceuticals in human and animals resulted in high environmental risks. Due to high cost-effectiveness, sulfamethoxazole (SMX) is one of the most widely used synthetic sulfonamides antibacterial agents to treat diseases and infections for human [3]. In addition, it is used for feed additives to promote growth rate and weight gain of food animals [4]. As a consequence, it has been frequently detected in various environmental matrices including soil, sediment, river, surface and ground water [5, 6].

Several remediation technologies such as adsorption [7, 8], ozonation [9], photolysis [10], chemical [3] and electrochemical oxidation [11] are available for elimination of SMX from various water bodies. Adsorption is considered as one of the practical options for removal of SMX mainly due to its simple operation,

no generation of harmful byproducts and cost-effectiveness [12]. Recently, adsorption of SMX on various materials has been investigated including clay minerals [13], graphene oxide [14], activated carbons (ACs) [15] and carbon nanotubes (CNTs) [1, 16]. Although some materials such as CNTs and graphene oxide have shown high adsorption capacities for SMX, high costs associated with manufacturing and disposal of these materials limited their practical application in fields [17].

As an alternative adsorbent, biochar (BC), which is a carbonaceous material (CM) produced by pyrolysis of biomass, has received enormous attention due to its low costs and adsorption of various contaminants [7]. Many BCs derived from paper mill sludge [18], bamboo [19], giant reed [8], herb-residue [20], crop straw [21], pine wood [22, 23] and anaerobically digested bagasse [24] have been applied to elimination of SMX. Unfortunately, these BCs showed the limited adsorption capacities for SMX (< 100 mg SMX/g BC). Therefore, possible activation and modification of raw BCs are suggested to enhance their adsorption capacity.



This is an Open Access article distributed under the terms of the Creative Commons Attribution Non-Commercial License (<http://creativecommons.org/licenses/by-nc/3.0/>) which permits unrestricted non-commercial use, distribution, and reproduction in any medium, provided the original work is properly cited.

Copyright © 2019 Korean Society of Environmental Engineers

Received October 10, 2018 Accepted December 1, 2018

† Corresponding author

Email: eunsung.kan@ag.tamu.edu

Tel: +1-254-968-4144 Fax: +1-254-968-3759

ORCID: 0000-0001-6298-6096

According to Thangalazhy-Gopakumar et al. [25], pine wood is one of the most abundant feedstock in the southern states in U.S. while making it an excellent precursor for BC. To date, a few studies have investigated the adsorption of SMX in water by the pine wood-derived BC (PBC) [22, 23]. However, these studies showed the limited adsorption capacities for SMX and have not investigated the detailed adsorption characteristics such as kinetic and isotherm modeling. The present study reports the detailed adsorption characteristics of pine wood-derived activated BC for SMX. This work also illustrated possible mechanisms for the adsorption of SMX onto the NaOH-activated PBC.

2. Materials and Methods

2.1. Reagents

All chemicals including SMX in the present study were purchased from Sigma-Aldrich Co. (Saint Louis, MO, USA) (Table 1). Based on the solubility of SMX in water at ambient conditions [26], 10-100 mg/L of SMX were used for the adsorption experiments in this study. Four commercial ACs used in the present study were obtained from Sigma-Aldrich Co. (Darco® G-60, Norit® GAC and Norit® GA1) and Calgon Carbon Corp. (Calgon F400).

2.2. Preparation of PBC

Pine wood (*Pinus taeda*) was used for production of PBC as reported in Jang et al. [27]. Briefly, the air-dried and sieved (20 mesh) pine wood was carbonized using the preheated pyrolysis furnace (MTI Corporation, Richmond, CA, USA) under 300°C for 15 min with 1 L/min of N₂ flow. The pristine PBC was designated as “R-PBC”.

2.3. Activation of PBC

Activation of R-PBC was carried out as follows: (1) Soaking 3 g of R-PBC in 40 mL of 4 M NaOH solution for 2 h at room temperature, (2) Pyrolyzing the dried NaOH-treated R-PBC under 800°C for 2 h with a heating rate of 3°C/min while maintaining oxygen limited conditions (2 L/min of N₂ flow), and (3) Washing the BC with 0.1 M HCl solution (200 mL) followed by a deionized (DI) water until the pH of BC reached 7.0. The washed and dried NaOH-activated PBC was designated as “A-PBC”.

2.4. Characterization of R- and A-PBCs

The physicochemical properties of the R- and A-PBCs were inves-

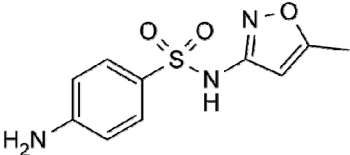
tigated in detail. Elemental composition analyzer (PerkinElmer 2400 Series II, MA, USA) and scanning electron microscope (SEM) (FEI Verios 460, Hillsboro, OR, USA) were used to evaluate the elemental compositions and the morphology, respectively. Thermogravimetric analysis (TA Instruments, New Castle, DE, USA) was used to evaluate the contents of fixed carbon, volatile compounds, and ash in R- and A-PBCs in accordance with ASTM standard D7582-15 [28]. Fourier transform infrared (FT-IR) spectroscopic analysis was conducted using a FT-IR spectrometer (Bruker Optik GmbH, Ettlingen, Germany). Brunauer-Emmett-Teller (BET) surface area and pore-size distribution were evaluated on the basis of the measurements relating to N₂ adsorption with an apparatus at 77 K (Micromeritics Gemini VII 2390p, Norcross, GA, USA). X-ray photoelectron spectroscopy (XPS) analysis was performed using XPS/UPS -SPECS System (SPECS Surface Nano Analysis GmbH, Berlin, Germany) equipped with a monochromatic Mg K α radiation to quantify carbon-oxygen functional groups. All spectra were acquired from a sample area of 1 mm \times 1 mm. The resolution of PHOIBOS 150 photoelectron analyzer is lower than 1 eV. The pH of zero point charges (pH_{PZC}) analysis was conducted as described previously [27]. Briefly, 0.01 M of 50 mL NaCl solution was used to maintain the ion strength and the initial pH of solution was adjusted ranged from 3.0 to 10.0. The final pH of solution was measured after 2 d incubation with 0.01 g of BC at 20°C and 150 rpm. The pH_{PZC} was calculated by the Δ pH = 0.

Energy loss spectroscopy (EELS) was conducted to analyze sp² content of the BCs (R- and A-PBCs). As described by Jang et al. [27], thin TEM samples of R- and A-PBCs were prepared by using UC7 Ultramicrotome (Leica Microsystems Inc. Buffalo Grove, IL, USA). Electron energy loss spectra for R- and A-PBCs were collected with the electron energy loss spectrometer (Gatan, Pleasanton, CA, USA) attached to probe aberration corrected scanning transmission electron Microscope (FEI Titan 80-300, Hillsboro, OR, USA). For further calculation, the carbon K-edge energy loss spectrum was deconvoluted into three Gaussian spectra [29].

The sp² content is defined as a relative value between the sample 1 s to π^* transition peak area ratio and that of graphite as calculated by Eq. (1) [30]:

$$SP^2 = \frac{\left[\frac{area(\pi^*)}{area(\pi^* + \sigma^*)} \right]_{sample}}{\left[\frac{area(\pi^*)}{area(\pi^* + \sigma^*)} \right]_{Graphite, reference}} \quad (1)$$

Table 1. Physical and Chemical Characteristics of Sulfamethoxazole (SMX)

Molecular structure	Formula	Molecular weight	Solubility ^a	pK _a
	C ₁₀ H ₁₁ N ₃ O ₃ S	253.28	0.37 g/L	pK ₁ = 1.6, pK ₂ = 5.7

^aAt ambient temperature [26].

where the transition at 285.0 eV indicates the electronic transition from carbon 1 s orbital to C = C π^* bonding orbital, the second transition at 292.0 eV indicates the electronic transition from carbon 1 s orbital to C - C σ^* bonding orbital, and the third transition at 298.0 eV indicates the electronic transition from carbon 1 s orbital to C = C σ^* bonding orbital [29, 31, 32].

2.5. Batch Adsorption Experiments

The effects of initial solution pH on adsorption of SMX was conducted at pH 1-10. Before mixing with the BCs, the solution pH was set to the desired pH by adding 0.1 M of HCl or NaOH solution. The foil covered glass bottles were agitated at 150 rpm and 20°C for 5 d. To quantitatively evaluate the contributions of individual SMX species to overall sorption at a tested pH value, the following empirical model was used (Eq. (2)) [33]:

$$K_d = K_d^- \alpha^- + K_d^0 \alpha^0 + K_d^+ \alpha^+ \quad (2)$$

where K_d (L/kg) is overall sorption coefficient and K_d^- , K_d^0 and K_d^+ are the sorption coefficients and α^- , α^0 and α^+ are the mass fraction for the SMX⁻, SMX⁰ and SMX⁺, respectively.

The adsorption kinetic study was conducted by stirring 0.01 g of A-PBC and 0.1 L of SMX solution (20 and 100 mg/L) at pH 4 which was determined as the optimum pH from the above experiments. The aqueous samples were taken at a regular interval for 2 d. In addition, the adsorption experiments for isotherm study were conducted by vigorously stirring 0.1 L of SMX solution (10 to 100 mg/L, pH 4) and 0.01 g of A-PBC for 5 d to reach equilibrium. The SMX concentration in water was evaluated and used for development of an appropriate isotherm model.

During the batch adsorption experiments, the samples were centrifuged and then filtered using a 0.45 μ m syringe filter. The concentration of SMX in filtrated solution was measured by a HPLC (LC-2030C model, SHIMADZU Corp., Torrance, CA, USA) with a C-18 column (Aeris PEPTIDE 3.6 μ m XB-C18, Phenomenex Inc., Torrance, CA, USA) and a UV-vis detector operating at wavelength of 265 nm. More detailed information about analysis of SMX by a HPLC was described in previously [27].

Adsorption capacity at time t , Q_t (mg/g) was calculated by Eq. (3):

$$Q_t = \frac{(C_0 - C_t) \times V}{M} \quad (3)$$

where C_0 and C_t are the SMX concentration of initial and at time t (mg/L), respectively, V is the volume of SMX solution (L) and M is the g of BC used in study.

The sum of squared error (SSE) was determined according to Eq. (4):

$$SSE = \sqrt{\frac{\sum (Q_e - Q_c)^2}{N}} \quad (4)$$

where Q_e and Q_c are the observed and calculated value of adsorp-

tion capacity (mg/g), respectively, and N is the number of measurements.

2.6. Adsorption Kinetic and Isotherm Models

The six adsorption kinetic models including pseudo-first order, pseudo-second order, Elovich, two-compartment first order, intra-particle diffusion and liquid film diffusion can be represented as follows (Eq. (5)-(10)):

$$\text{Pseudo-first order (PFO): } Q_t = Q_e (1 - \exp(-K_1 t)) \quad (5)$$

$$\text{Pseudo-second order (PSO): } Q_t = \frac{K_2 Q_e^2 t}{1 + K_2 Q_e t} \quad (6)$$

$$\text{Elovich: } Q_t = \left(\frac{1}{b}\right) \ln ab + \left(\frac{1}{b}\right) \ln t, \quad t_0 = \frac{1}{ab} \quad (7)$$

$$\text{Intra-particle diffusion: } Q_t = K_i \sqrt{t} + C_i \quad (8)$$

$$\text{Liquid file diffusion: } \ln(1 - F) = -K_{fd} t, \quad F = \frac{Q_t}{Q_e} \quad (9)$$

Two-compartment first order:

$$\frac{Q_t}{Q_{t=\infty}} = F_{fast} (1 - \exp^{-tK_{fast}}) + F_{slow} (1 - \exp^{-tK_{slow}}) \quad (10)$$

where Q_e = adsorption capacity (mg/g) at equilibrium time, Q_t = adsorption capacity (mg/g) at time t (min), K_1 = rate constant of pseudo-first order, K_2 = rate constant of pseudo-second order, a = rate constant of chemisorption, b = constant of the surface coverage, K_i = intra-particle diffusion rate constant (mg·min^{0.5}/g), C_i = a constant (mg/g), K_{fd} = adsorption rate constant, F_{fast} = mass fraction of fast, F_{slow} = mass fraction of slow, K_{fast} = first order rate constant for transfer into fast (h⁻¹), K_{slow} = first order rate constant for transfer into slow (h⁻¹), h = hour.

In this study, three isotherm models including Langmuir, Freundlich and Temkin models were used to fit the experimental data (Eq. (11)-(13)):

$$\text{Langmuir: } Q_e = \frac{Q_m K_L C_e}{1 + K_L C_e}, \quad R_L = \frac{1}{1 + K_L C_0} \quad (11)$$

$$\text{Freundlich: } Q_e = K_f C_e^{1/n_f} \quad (12)$$

$$\text{Temkin: } Q_e = \frac{RT}{b_T} \ln(K_T C_e) \quad (13)$$

Where Q_e = adsorption capacity (mg/g) at equilibrium time, Q_m = maximum adsorption capacity (mg/g), K_L = Langmuir constant, C_e = equilibrium concentration (mg/L), R_L = separation constant, K_f and n_f = Freundlich constant, R = universal gas constant (8.314 J/mol), T = temperature in terms of Kelvin, b_T = Temkin constant, K_T = equilibrium bond constant related to the maximum energy of bond, t = time (min).

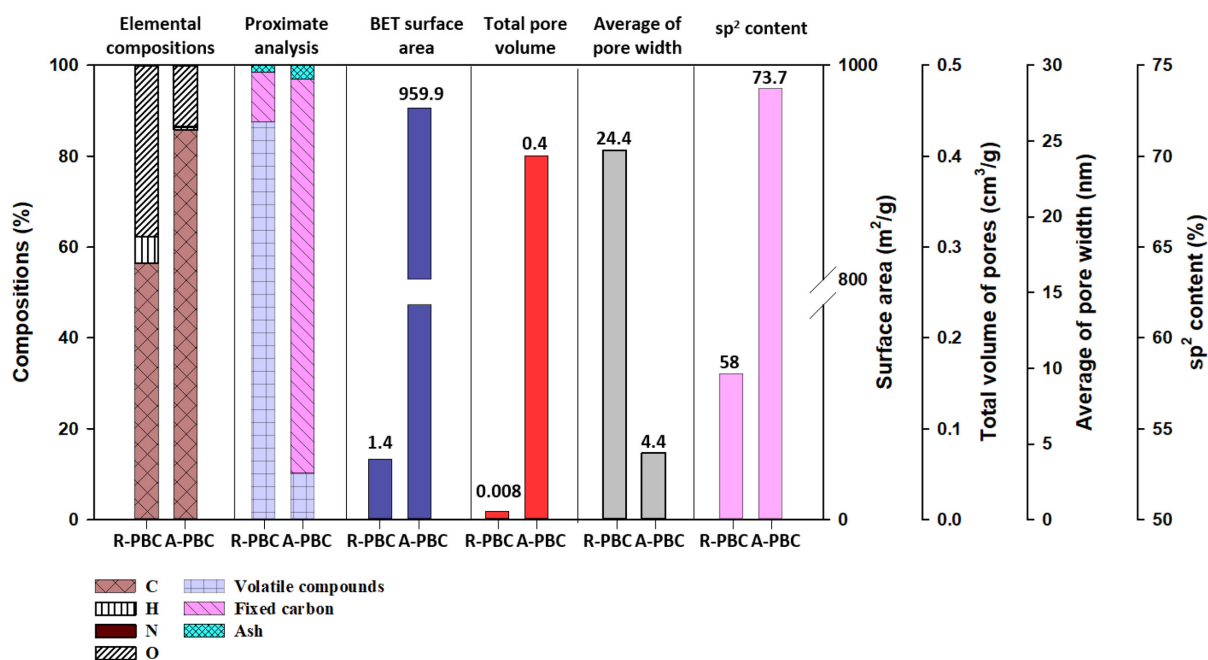


Fig. 1. Physical, chemical and textual characteristics of R- and A-PBCs.

3. Results and Discussion

3.1. Effect of Activation on Physicochemical Properties of BC

The physicochemical properties of R-PBC and A-PBC are presented in Fig. 1. For the elemental compositions, the C content increased from 56.4 to 85.8% after activation, whereas the O and H contents decreased from 37.6 to 13.5% and from 5.9 to 0.5%, respectively. With decomposition of O and H under high temperature [27], significant structural changes occurred in A-PBC. As shown in Fig. 2, the ratio of O/C decreased from 0.67 to 0.16 while the ratio of H/C decreased from 0.10 to 5.8×10^{-3} , respectively. The decrease in the ratios of O/C and H/C represented decarboxylation (i.e., loss of CO_2) and demethylation (i.e., loss of CH_3) [34], respectively, suggesting the formation of porous polyaromatic structures with rich carbon content after the NaOH activation of R-PBC. Interestingly, the O/C and H/C of A-PBC were lower than those of other BCs made from grasses, crop residues, manure and sewage sludge, but were close to that of powder activated carbon (Fig. 2). The low O/C and H/C of A-PBC indicated high hydrophobicity and aromaticity in A-PBC which would be closely related to adsorption characteristics of A-PBC for hydrophobic contaminants.

Fig. 1 showed the calculated sp^2 content of R-PBC and A-PBC. Interestingly, A-PBC showed higher sp^2 content (73.7%) than that of R-PBC (58.0%). Similarly, Yoo et al. [30] reported the increase in sp^2 content as a function of pyrolysis temperature during the pyrolysis of pine wood. Thus, the increase in sp^2 content in A-PBC might be due to the increase in pyrolysis temperature (800°C) during NaOH activation of R-PBC. Also, this was consistent with ^{13}C DP/NMR data (i.e. a growing aromatic structure after NaOH activation of pine BC) which reported by Park et al. [35].

Furthermore, FTIR spectrum of A-PBC exhibited the negligible functional groups and more similar to commercial ACs which have high hydrophobicity (Fig. S1).

After NaOH activation, changes in the morphology of BC surface were observed (Fig. S2). The sponge-like structure in A-PBC indicated the development of micro/meso-pore on the surface. This is highly supported by the data from the textural analysis (i.e., decreased in average of pore width and increased in volume of

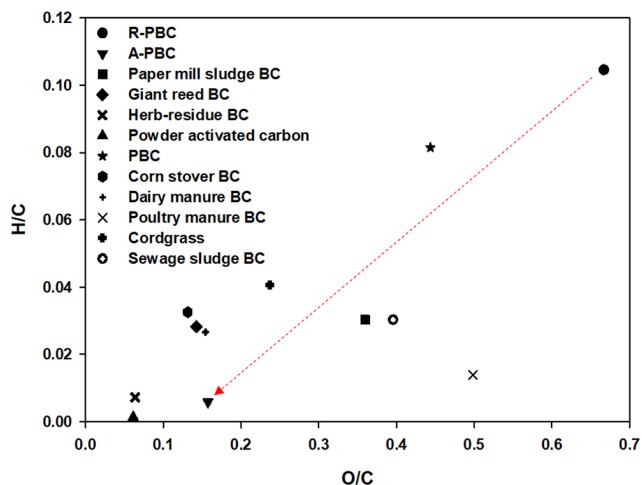


Fig. 2. Van Krevelen plot of elemental ratios for R- and A-PBCs. Other BCs or ACs derived from paper mill sludge [18], giant reed [8], herb-residue [20], powered ACs [23], corn stover, dairy manure, poultry manure [47], cordgrass, pine wood [48] and sewage sludge [49] were used to fit in this study. Red arrow indicates the change in properties between R- and A-PBC.

pores) (Fig. 1). With the well-developed structure, high BET surface area (959.9 m²/g) was achieved in A-PBC. Thus, the activation of PBC increased hydrophobicity and surface area which can lead to more heterogeneous adsorption characteristics [21, 36].

3.2. Effects of Initial pH on Adsorption Capacity

Recently, a strong relationship between SMX species and surface charge of CMs has been reported in the literatures [8, 37]. To take the SMX property into consideration, adsorption capacities (Q_e , mg/g) of SMX on the R-PBC and A-PBC were investigated at various initial solution pH (Fig. 3). Both BCs exhibited similar pH-dependent adsorption patterns. The Q_e values increased with increasing pH from 1 to 4 and then reached the maximum at pH 4 for both BCs (58.91 mg/g for R-PBC and 437.36 mg/g for A-PBC). Meanwhile, the significantly decreased Q_e values were observed at pH higher than 7. Similar results were found from the pH-dependent SMX adsorption on bamboo-derived BC [19].

The higher K_d^0 than both K_d^+ and K_d^- at the pH of 2-5 (for R-PBC) and 1-6 (for A-PBC) was observed in both R-PBC and A-PBC (Table S1), indicating the importance of SMX⁰ species to the overall adsorption. At the pH ranges between 1 and 5, the contribution of SMX⁰ species to the overall adsorption was higher than 51% (Fig. S3). This was consistent with the data from Zheng *et al.* [8] who reported significant contribution of SMX⁰ species to the overall adsorption on giant reed BC. Interestingly, between pH 1 and 5, the contribution of SMX⁰ species to the overall adsorption on A-PBC was higher than that of R-PBC, suggesting that activation process enhanced hydrophobic interaction as well π - π interaction which was predominant adsorption mechanisms for SMX species on A-PBC [16, 38].

As shown in Fig. 3, the SMX⁺ and SMX⁻ are the dominant species at pH < pK_{a1} = 1.6 and pH > pK_{a2} = 5.7, respectively, and SMX⁰ is dominant at pH between pK_{a1} and pK_{a2}. In addition, it is assumed that the surface charge of BC was protonated (*i.e.*, positive charge) when the solution pH was lower than the pH_{ZPC} of

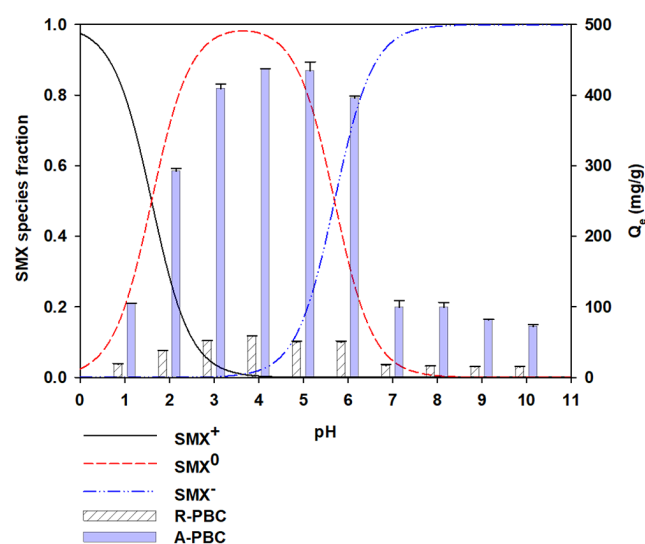


Fig. 3. pH-dependent SMX species and adsorption capacities of R- and A-PBCs.

BC, otherwise it was the negative. Considering the pH_{ZPC} of R-PBC (5.08) and A-PBC (6.83) (Table S1), a strong electrostatic repulsion between the SMX species and surface of BCs would occur at high pH (> 7) or low pH (< 1) resulting in relatively low value of Q_e . However, it is interesting to note that some portion of SMX (72-98 mg/g) was still adsorbed on the A-PBC at high pH (> 7), although a strong electrostatic repulsion would be expected between the SMX⁻ and negative charged surface of BCs. This was explained by a strong negative charged assistant hydrogen bond (CAHB) along with oxygen-containing group on surface [20]. Teixidó *et al.* [33] and Yu *et al.* [16] reported that -NH₂ and -SO₂NH- groups in sulfonamides can interact with oxygen-containing group on surface of CMs. Thus, it is hypothesized that A-PBC has a high potential for hydrogen bonding accepting or donating due to its plenty of oxygen-containing group on surface of A-PBC (Table S1). As expected, the significant decrease in Q_e values (about 291 mg/g at pH 2 and 104 mg/g at pH 1) were also observed at low pH due to the much less hydrophobicity of A-PBC with abundant ionized forms and the inhibited Lewis acid-base interaction [1].

π - π electron donor-acceptor (EDA) interaction is one of the possible mechanisms for the adsorption of sulfonamides on BC surface [19, 39]. SMX has a strong π -electron acceptor nature due to its *p*-amino rings (donates lone pair electrons to the benzene ring) and N and/or O-hetero-aromatic rings (contribution to electronic resonance), while the graphite structure π -electron of BC can act as electron donor [16, 19]. The ability for π - π EDA interaction of different SMX species follows the order of SMX⁺ > SMX⁰ > SMX⁻ due to the decrease in π -withdrawing ability resulted from deprotonation of -SO₂NH- groups [40], while increased by protonation of -NH₂- groups [41]. At pH ranges between 4 and 6, this was not consistent with the order of K_d ($K_d^0 > K_d^- > K_d^+$) in this study. Thus, π - π EDA interaction was not the major mechanism for adsorption of SMX onto A-PBC at these pH ranges. This was also consistent with the previous research [16] which reported the strong hydrophobic interaction between TC and CNTs rather than π - π EDA interaction. In contrast, previous researches [42, 43] reported the possible π - π EDA interaction between SMX and CMs. Recently, Yoo [44] reported the increasing π - π^* transition (plasmon) intensity after the chemical activation of PBC. Similarly, Peng *et al.* [45] reported that adsorption is determined mainly by the number or areas of aromatic rings in both antibiotics and adsorbent when the main adsorption mechanism is the π - π interaction. Collectively, it is reasonable to conclude that the A-PBC in this study with the high surface area (959.9 m²/g), hydrophobicity and sp² after the NaOH activation resulted in high SMX adsorption capacity via possible adsorption mechanisms including hydrophobic interaction, π - π EDA interaction and hydrogen bonding.

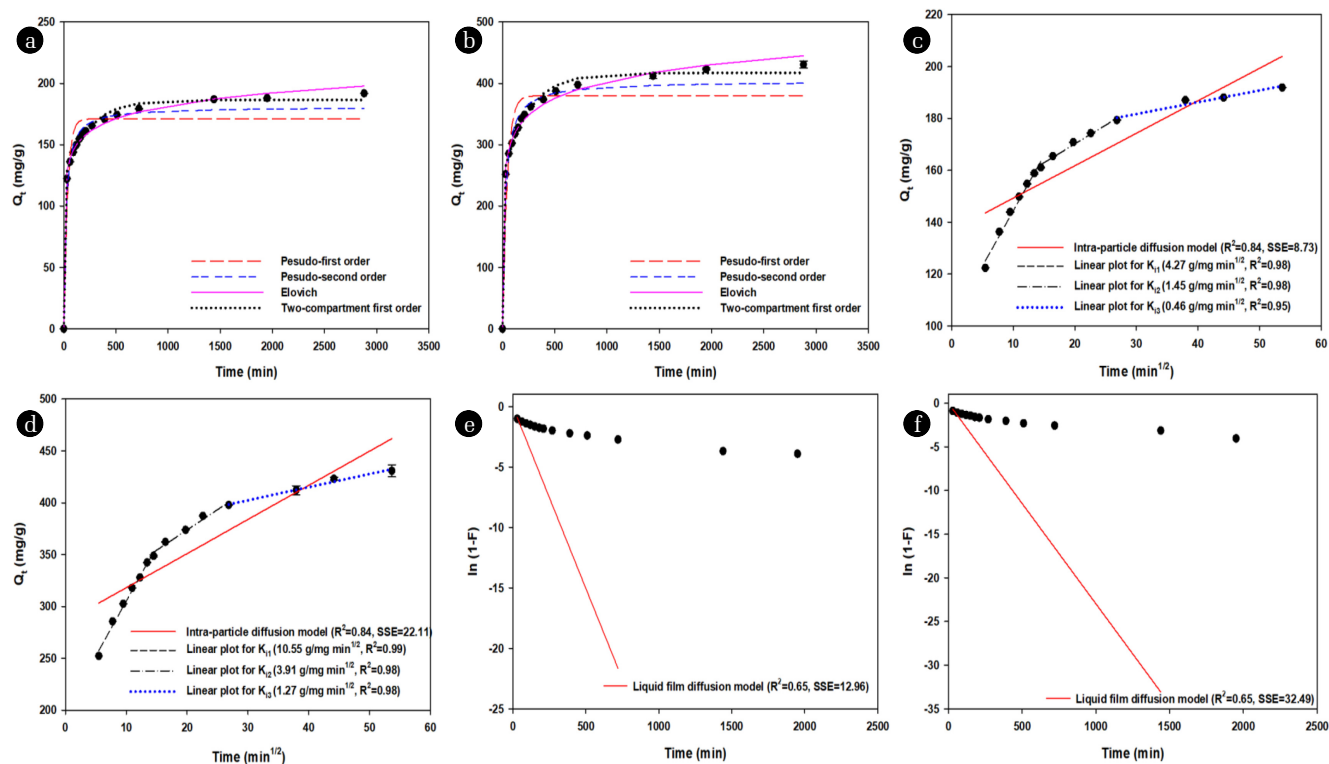
3.3. Adsorption Kinetics and Isotherms

To understand the possible adsorption mechanisms and rate-limiting step, the kinetic study for adsorption of SMX onto A-PBC was conducted as described in section 2.5 (Fig. 4). Investigation of adsorption kinetics of SMX and A-PBC interaction using PFO, PSO, Elovich and two-compartment first order are summarized

Table 2. Summary of Kinetic Parameters of SMX Adsorption on A-PBC

	Pseudo-first order					Pseudo-second order			
	Q_e^b	Q_e^c	K_1	SSE	R^2	Q_e^b	K_2	SSE	R^2
20 ^a	191.93	171.08	0.03	12.96	0.65	179.69	2.89×10^{-4}	5.54	0.92
100 ^a	430.82	380.13	0.03	32.49	0.65	400.30	9.74×10^{-5}	14.3	0.91

	Elovich				Two-compartment first order								
	Q_e^c	a	b	t_0	SSE	R^2	Q_e^c	F_{fast}	F_{slow}	K_{fast}	K_{slow}	SSE	R^2
20 ^a	197.79	2.43×10^3	0.07	6.22×10^{-3}	3.25	0.98	186.56	0.8281	0.1719	163.7	0.26	3.18	0.98
100 ^a	445.08	1.05×10^3	0.03	3.78×10^{-2}	7.96	0.98	417.11	0.8475	0.1525	116.16	0.25	7.38	0.98

^aInitial concentration of SMX (mg/L)^bObserved value^cCalculated value**Fig. 4.** Adsorption kinetic of SMX on A-PBC by fitting the pseudo-first order, pseudo-second order, Elovich and two-compartment first order ((a) and (b)), intra-particle model ((c) and (d)) and film diffusion model ((e) and (f)). Two different initial concentration 20 mg/L for (a), (c) and (e) and 100 mg/L for (b), (d) and (f).

in Table 2. Most of studies reported that kinetic data from sulfonamides adsorption experiment was well-fitted by PSO indicating chemisorptive interaction [7]. As shown in Fig. 4 and Table 2, PSO (R^2 of 0.91-0.92) was more suitable than PFO (R^2 of 0.65) to describe the interaction between SMX and A-PBC. In addition, Elovich was the best fitted kinetic model with lowest SSE (3.25-7.96) and highest R^2 (0.98) suggesting that strong chemisorptive interaction occurred on energetically heterogeneous surface of A-PBC [46].

Additionally, the time-courses of SMX adsorption data was analyzed using a two-compartment first order model (Fig. 4(a) and (b)). This model well fitted the dynamics of SMX (20 and

100 mg/L) on A-PBC with low SSE (3.18-7.38) and high R^2 (0.98). The significantly higher F_{fast} (0.83-0.85) and K_{fast} (116.16-163.7) value than those of F_{slow} (0.15-0.17) and K_{slow} (0.25-0.26), indicating that the fast sorption stage was predominant during adsorption process. This was supported by the calculated values from Elovich model (i.e. the higher a (adsorption rate) than b (desorption rate)).

In general, transfer of solutes to adsorbents is usually characterized by liquid film diffusion or intraparticle diffusion. In this study, two diffusion models (intra-particle diffusion and film diffusion) were used to gain insight into the rate-limiting steps affecting the kinetics of SMX adsorption onto A-PBC. As shown in Fig. 4(c)-(f), intra-particle diffusion model was more fitted (R^2 of 0.84)

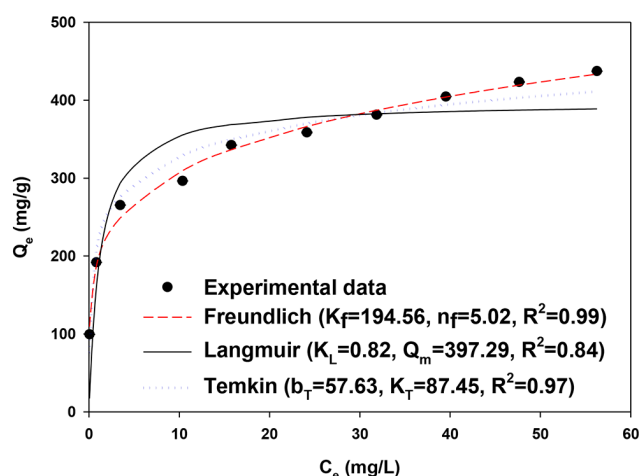


Fig. 5. Adsorption isotherms of SMX on A-PBC by fitting the Freundlich, Langmuir and Temkin models.

to the experimental results than liquid film model (R^2 of 0.65). Thus, intra-particle diffusion would be considered as the major limitation for the adsorption of SMX onto A-PBC. More detailed corresponding rate constants (i.e., K_{i1} - K_{i3}) (Fig. 4(c) and (d)) derived from linear regression represented the highest constant at the first stage (4.27-10.55 g/mg min^{1/2}), while rate constants of 2nd (1.45-3.91 g/mg min^{1/2}) and 3rd stages (0.46-1.27 g/mg min^{1/2}) attributed to the intra-particle diffusion showed low value. Especially, the rate constants of 3rd stage assigned to micropore diffusion was significantly lower than those of the previous two stages. This phenomenon is frequently observed during adsorption of

organic contaminants resulted from decreased active adsorption sites on BCs [46].

Several literatures reported that isotherms of SMX adsorption onto various BCs could be fitted into either Langmuir [21] or Freundlich [8, 18-20] model. Based on the type of isotherm of A-PBC (i.e., Type I) (Fig. 5), three phenomenological models including Langmuir (no decrease of heat), Freundlich (a logarithmic decrease of heat) and Temkin (a linear decrease of heat) were applied in this study. The results in Fig. 5 showed Freundlich model was more appropriate than Langmuir and Temkin models indicating that the adsorption may take place on a heterogeneous surface with varied affinities. Based on the n_f values derived from Freundlich model, the adsorption of SMX was favorable (i.e. the n_f value within the range 1-10) onto A-PBC with high energetic heterogeneity. Besides, when the results from the isotherm experiments were fitted to Langmuir and Temkin models, the Langmuir constant ($K_L = 0.82$) and Temkin constant ($b_T = 57.63$) suggested the SMX adsorption onto A-PBC would be favorable (i.e., $0 < R_L < 1$) and adsorption reaction would occur exothermically (i.e., $b_T > 1$) in the concentration range used in this study.

3.4. Comparison of the SMX Adsorption Capacities of Various CMs

Table 3 lists the maximum adsorption capacities for SMX and surface areas of CMs. The Q_m value for A-PBC (397.29 mg/g) was higher than those of various CMs including BC, AC, CNT and graphene oxide. For example, Zheng *et al.* [8] and Sun *et al.* [21] reported the Q_m value of 1.93-4.99 mg/g and 0.25-7.40

Table 3. Maximum Adsorption Capacity (Q_m) of SMX and the Surface Area of Various CMs

Carbonaceous materials	Surface area (m ² /g)	Q_m (mg/g)	References
Giant reed BC (300°C)	2.09	4.99 ^b	Zheng <i>et al.</i> [8]
Giant reed BC (600°C)	58.75	1.93 ^b	
Bamboo BC (H ₃ PO ₄ activated, 600°C)	1.12	88.10 ^b	Ahmed <i>et al.</i> [19]
Rice-straw BC (300°C)	5.76	4.21 ^b	Sun <i>et al.</i> [21]
Rice-straw BC (600°C)	27.4	7.40 ^b	
Wheat-straw BC (300°C)	7.62	6.75 ^b	
Wheat-straw BC (600°C)	38.1	0.25 ^b	
Primary paper mill sludge BC (800°C)	209.12	1.69 ^b	Calisto <i>et al.</i> [18]
Commercial AC (ChemViron Carbon)	848.22	118 ^b	
Anaerobically digested bagasse BC (600°C)	17.66 ^c	54.38 ^b	Yao <i>et al.</i> [24]
Graphene Oxide	-	240 ^b	Chen <i>et al.</i> [14]
Coal based AC (Norit®)	851	185.19 ^b	Çalışkan and Göktürk [15]
Multi-walled CNTs	382	71.8 ^b	
R-PBC	1.4	58.91 ^a	Zhao <i>et al.</i> [1]
A-PBC	959.9	437.36 ^a , 397.29 ^b	
Commercial AC (Calgon F400)	816.3 ^d	312.14 ^a	In this study
Commercial AC (Darco® G-60)	933 ^e	328.83 ^a	
Commercial AC (Norit® CA1)	980 ^f	399.94 ^a	
Commercial AC (Norit® GAC)	1,200 ^f	377.5 ^a	

^a Derived from experimental data; ^b Derived from isotherm model data; ^c [50]; ^d [51]; ^e [52]; ^f [53]

mg/g using the BCs from giant reed and crop residues, respectively. In addition, Çalışkan and Göktürk [15] and Chen et al. [14] achieved the Q_m value of 185.19 mg/g and 240 mg/g using commercial AC and graphene oxide, respectively. From the statistical results (i.e., Pearson correlation) (Fig. S4), the listed surface area showed positive correlation ($r = 0.904$, $p < 0.01$) with Q_m value, suggesting that high SMX adsorption capacity on A-PBC could be attributed to its highly increased surface area (959.9 m²/g) with well-developed porous structure after activation.

To evaluate the feasibility of PBC for adsorption of SMX, the batch adsorption experiments were conducted using four commercial ACs (Calgon F400, Darco® G-60, Norit® CA1 and Norit® GAC) under the same conditions (0.1 g/L, 100 mg/L of SMX and pH 4). As shown in Table 3, the Q_m of A-PBC (397.29 mg/g) was comparable to four commercial ACs (312.14 mg/g for Calgon F400, 328.83 mg/g for Darco® G-60, 377.5 mg/g for Norit® GAC and Norit® CA1 for 399.94 mg/g). Thus, these results supported the A-PBC would have high potential for removal of SMX in wastewater and water after process optimization.

Recently, Ahmed et al. [19] reported that adsorption of SMX onto BCs decreased when containing competing compounds (i.e., sulfamethazine and sulfathiazole) while it was enhanced with low molecular weight organic acids (e.g., citric- and malic acid) [21]. Thus, further investigations will include adsorption of SMX onto A-PBC in various wastewater containing multiple contaminants. In addition, appropriate regeneration processes (e.g., chemical VS thermal) of the A-PBC should be studied to increase their cost effectiveness.

4. Conclusions

The NaOH-activated PBC (A-PBC) was prepared and it showed highest adsorption capacity for SMX at pH 4 at which SMX (mostly neutral form of SMX) would be adsorbed onto A-PBC via mainly π - π and hydrophobic interactions. The kinetic studies showed the Elovich and intraparticle diffusion models were the most appropriate ones indicating the chemisorption of SMX onto surface of A-PBC with diffusion limitation. The Freundlich model was found to be best fitted isotherm model indicating heterogeneous and multiple layer of adsorption. A-PBC demonstrated its high adsorption capacity for SMX which was comparable with commercial ACs.

Acknowledgments

This work was funded by Texas A&M University Chancellor Research Initiative Fund and the US-DOE Office of Energy Efficiency and Renewable Energy (Award Number DE-EE0006639).

References

- Zhao H, Liu X, Cao Z, et al. Adsorption behavior and mechanism of chloramphenicols, sulfonamides, and non-antibiotic pharmaceuticals on multi-walled carbon nanotubes. *J. Hazard. Mater.* 2016;310:235-245.
- Kümmerer K. The presence of pharmaceuticals in the environment due to human use – Present knowledge and future challenges. *J. Environ. Manage.* 2009;90:2354-2366.
- Qi C, Liu X, Lin C, et al. Degradation of sulfamethoxazole by microwave-activated persulfate: Kinetics, mechanism and acute toxicity. *Chem. Eng. J.* 2014;249:6-14.
- Kumar A, Xagorarakis I. Pharmaceuticals, personal care products and endocrine-disrupting chemicals in US surface and finished drinking waters: A proposed ranking system. *Sci Total Environ.* 2010;408:5972-5989.
- Liu J-L, Wong M-H. Pharmaceuticals and personal care products (PPCPs): A review on environmental contamination in China. *Environ. Int.* 2013;59:208-224.
- Luo Y, Xu L, Rysz M, Wang Y, Zhang H, Alvarez PJ. Occurrence and transport of tetracycline, sulfonamide, quinolone, and macrolide antibiotics in the Haihe River Basin, China. *Environ. Sci. Technol.* 2011;45:1827-1833.
- Peiris C, Gunatilake SR, Mlsna TE, Mohan D, Vithanage M. Biochar based removal of antibiotic sulfonamides and tetracyclines in aquatic environments: A critical review. *Bioresour. Technol.* 2017;246:150-159.
- Zheng H, Wang Z, Zhao J, Herbert S, Xing B. Sorption of antibiotic sulfamethoxazole varies with biochars produced at different temperatures. *Environ. Pollut.* 2013;181:60-67.
- Akhtar J, Amin NS, Aris A. Combined adsorption and catalytic ozonation for removal of sulfamethoxazole using Fe₂O₃/CeO₂ loaded activated carbon. *Chem. Eng. J.* 2011;170:136-144.
- Boreen AL, Arnold WA, McNeill K. Photochemical fate of sulfa drugs in the aquatic environment: Sulfa drugs containing five-membered heterocyclic groups. *Environ. Sci. Technol.* 2004;38:3933-3940.
- de Amorim KP, Romualdo LL, Andrade LS. Electrochemical degradation of sulfamethoxazole and trimethoprim at boron-doped diamond electrode: Performance, kinetics and reaction pathway. *Sep. Purif. Technol.* 2013;120:319-327.
- Putra EK, Pranowo R, Sunarso J, Indraswati N, Ismadji S. Performance of activated carbon and bentonite for adsorption of amoxicillin from wastewater: Mechanisms, isotherms and kinetics. *Water Res.* 2009;43:2419-2430.
- Gao J, Pedersen JA. Adsorption of sulfonamide antimicrobial agents to clay minerals. *Environ. Sci. Technol.* 2005;39:9509-9516.
- Chen H, Gao B, Li H. Removal of sulfamethoxazole and ciprofloxacin from aqueous solutions by graphene oxide. *J. Hazard. Mater.* 2015;282:201-207.
- Çalışkan E, Göktürk S. Adsorption characteristics of sulfamethoxazole and metronidazole on activated carbon. *Sep. Sci. Technol.* 2010;45:244-255.
- Yu X, Zhang L, Liang M, Sun W. pH-dependent sulfonamides adsorption by carbon nanotubes with different surface oxygen contents. *Chem. Eng. J.* 2015;279:363-371.
- Tabish TA, Memon FA, Gomez DE, Horsell DW, Zhang S. A facile synthesis of porous graphene for efficient water and wastewater treatment. *Sci. Rep.* 2018;8:1817.
- Calisto V, Ferreira CI, Oliveira JA, Otero M, Esteves VI. Adsorptive removal of pharmaceuticals from water by com-

- mercial and waste-based carbons. *J. Environ. Manage.* 2015;152:83-90.
19. Ahmed MB, Zhou JL, Ngo HH, Guo W, Johir MAH, Somalingam K. Single and competitive sorption properties and mechanism of functionalized biochar for removing sulfonamide antibiotics from water. *Chem. Eng. J.* 2017;311:348-358.
 20. Lian F, Sun B, Song Z, Zhu L, Qi X, Xing B. Physicochemical properties of herb-residue biochar and its sorption to ionizable antibiotic sulfamethoxazole. *Chem. Eng. J.* 2014;248:128-134.
 21. Sun B, Lian F, Bao Q, Liu Z, Song Z, Zhu L. Impact of low molecular weight organic acids (LMWOAs) on biochar micropores and sorption properties for sulfamethoxazole. *Environ. Pollut.* 2016;214:142-148.
 22. Xie M, Chen W, Xu Z, Zheng S, Zhu D. Adsorption of sulfonamides to demineralized pine wood biochars prepared under different thermochemical conditions. *Environ. Pollut.* 2014;186:187-194.
 23. Shimabuku KK, Kearns JP, Martinez JE, Mahoney RB, Moreno-Vasquez L, Summers RS. Biochar sorbents for sulfamethoxazole removal from surface water, stormwater, and wastewater effluent. *Water Res.* 2016;96:236-245.
 24. Yao Y, Zhang Y, Gao B, Chen R, Wu F. Removal of sulfamethoxazole (SMX) and sulfapyridine (SPY) from aqueous solutions by biochars derived from anaerobically digested bagasse. *Environ. Sci. Pollut. Res.* 2018;25:25659-25667.
 25. Thangalazhy-Gopakumar S, Adhikari S, Ravindran H, et al. Physicochemical properties of bio-oil produced at various temperatures from pine wood using an auger reactor. *Bioresour. Technol.* 2010;101:8389-8395.
 26. Martínez F, Gómez A. Estimation of the solubility of sulfonamides in aqueous media from partition coefficients and entropies of fusion. *Phys. Chem. Liq.* 2002;40:411-420.
 27. Jang HM, Yoo S, Choi Y-K, Park S, Kan E. Adsorption isotherm, kinetic modeling and mechanism of tetracycline on Pinus taeda-derived activated biochar. *Bioresour. Technol.* 2018;259:24-31.
 28. ASTM. Standard test methods for proximate analysis of coal and coke by macro thermogravimetric analysis. West Conshohocken: ASTM International; 2016.
 29. Marriott A, Hunt A, Bergström E, et al. Investigating the structure of biomass-derived non-graphitizing mesoporous carbons by electron energy loss spectroscopy in the transmission electron microscope and X-ray photoelectron spectroscopy. *Carbon* 2014;67:514-524.
 30. Yoo S, Kelley SS, Tilotta DC, Park S. Structural characterization of loblolly pine derived biochar by X-ray diffraction and electron energy loss spectroscopy. *ACS Sustain. Chem. Eng.* 2018;6:2621-2629.
 31. Zhang Z-L, Brydson R, Aslam Z, et al. Investigating the structure of non-graphitising carbons using electron energy loss spectroscopy in the transmission electron microscope. *Carbon* 2011;49:5049-5063.
 32. Daniels H, Brydson R, Rand B, Brown A. Investigating carbonization and graphitization using electron energy loss spectroscopy (EELS) in the transmission electron microscope (TEM). *Philos. Mag.* 2007;87:4073-4092.
 33. Teixidó M, Pignatello JJ, Beltrán JL, Granados M, Peccia J. Speciation of the ionizable antibiotic sulfamethazine on black carbon (biochar). *Environ. Sci. Technol.* 2011;45:10020-10027.
 34. Zhu X, Liu Y, Zhou C, Luo G, Zhang S, Chen J. A novel porous carbon derived from hydrothermal carbon for efficient adsorption of tetracycline. *Carbon* 2014;77:627-636.
 35. Park J, Hung I, Gan Z, Rojas OJ, Lim KH, Park S. Activated carbon from biochar: Influence of its physicochemical properties on the sorption characteristics of phenanthrene. *Bioresour. Technol.* 2013;149:383-389.
 36. Keiluweit M, Nico PS, Johnson MG, Kleber M. Dynamic molecular structure of plant biomass-derived black carbon (biochar). *Environ. Sci. Technol.* 2010;44:1247-1253.
 37. Ji L, Liu F, Xu Z, Zheng S, Zhu D. Adsorption of pharmaceutical antibiotics on template-synthesized ordered micro- and mesoporous carbons. *Environ. Sci. Technol.* 2010;44:3116-3122.
 38. Ji L, Chen W, Duan L, Zhu D. Mechanisms for strong adsorption of tetracycline to carbon nanotubes: A comparative study using activated carbon and graphite as adsorbents. *Environ. Sci. Technol.* 2009;43:2322-2327.
 39. Chen W, Duan L, Wang L, Zhu D. Adsorption of hydroxyl- and amino-substituted aromatics to carbon nanotubes. *Environ. Sci. Technol.* 2008;42:6862-6868.
 40. Ji L, Chen W, Zheng S, Xu Z, Zhu D. Adsorption of sulfonamide antibiotics to multiwalled carbon nanotubes. *Langmuir* 2009;25:11608-11613.
 41. Hansch C, Leo A, Taft R. A survey of Hammett substituent constants and resonance and field parameters. *Chem. Rev.* 1991;91:165-195.
 42. Reguyal F, Sarmah AK. Adsorption of sulfamethoxazole by magnetic biochar: Effects of pH, ionic strength, natural organic matter and 17 α -ethinylestradiol. *Sci. Total Environ.* 2018;628:722-730.
 43. Chen H, Gao B, Li H. Functionalization, pH, and ionic strength influenced sorption of sulfamethoxazole on graphene. *J. Environ. Chem. Eng.* 2014;2:310-315.
 44. Yoo S. Structural characterizations of biomass-derived carbon materials and application as supercapacitor electrode [dissertation]. USA: North Carolina State Univ.; 2018.
 45. Peng B, Chen L, Que C, et al. Adsorption of antibiotics on graphene and biochar in aqueous solutions induced by π - π interactions. *Sci. Rep.* 2016;6:31920.
 46. Zhou Y, Liu X, Xiang Y, et al. Modification of biochar derived from sawdust and its application in removal of tetracycline and copper from aqueous solution: Adsorption mechanism and modelling. *Bioresour. Technol.* 2017;245:266-273.
 47. Enders A, Hanley K, Whitman T, Joseph S, Lehmann J. Characterization of biochars to evaluate recalcitrance and agronomic performance. *Bioresour. Technol.* 2012;114:644-653.
 48. Harvey OR, Herbert BE, Rhue RD, Kuo L-J. Metal interactions at the biochar-water interface: Energetics and structure-sorption relationships elucidated by flow adsorption microcalorimetry. *Environ. Sci. Technol.* 2011;45:5550-5556.
 49. Yang X, Xu G, Yu H, Zhang Z. Preparation of ferric-activated sludge-based adsorbent from biological sludge for tetracycline removal. *Bioresour. Technol.* 2016;211:566-573.
 50. Inyang M, Gao B, Pullammanappallil P, Ding W, Zimmerman AR. Biochar from anaerobically digested sugarcane bagasse.

- Bioresour. Technol.* 2010;101:8868-8872.
51. Gauden PA, Szmechtig-Gauden E, Rychlicki G, Duber S, Garbacz JK, Buczkowski R. Changes of the porous structure of activated carbons applied in a filter bed pilot operation. *J. Colloid Interface Sci.* 2006;295:327-347.
52. Oliveira LCA, Rios RVRA, Fabris JD, Garg V, Sapag K, Lago RM. Activated carbon/iron oxide magnetic composites for the adsorption of contaminants in water. *Carbon* 2002;40:2177-2183.
53. Gicheva G, Yordanov G. Removal of citrate-coated silver nanoparticles from aqueous dispersions by using activated carbon. *Colloids Surf. A* 2013;431:51-59.